Eur. Phys. J. Special Topics **224**, 341–354 (2015)

DOI: 10.1140/epjst/e2015-02364-4

THE EUROPEAN PHYSICAL JOURNAL SPECIAL TOPICS

Regular Article

Free surface flow simulation with application to bluff body flow control

S. Kocabiyik[1,a] and C. Bozkaya[2]

[1] Department of Mathematics and Statistics, Memorial University of Newfoundland, St. John's, NL, A1C 5S7, Canada
[2] Department of Mathematics, Middle East Technical University, Ankara 06800, Turkey

Received 30 July 2014 / Received in final form 16 February 2015
Published online 8 April 2015

Abstract. To better understand the interaction of a free surface wave motion with moving bluff bodies, a two-dimensional numerical study of the forced streamwise oscillation of a circular cylinder beneath a free surface is conducted based on a two-fluid model. Computations are carried out at a Reynolds number of $R = 200$, a fixed displacement amplitude, $A = 0.13$ and the forcing frequency-to-natural shedding frequency ratios, $f/f_0 = 1.5, 2.5, 3.5$. Finite volume discretization of the special integral form of two-dimensional continuity and unsteady Navier-Stokes equations (when a solid body is present) are performed on a fixed Cartesian grid. Improved volume-of-fluid method is used to discretize the free surface. The laminar asymmetric flow regimes in the near wake region and the fluid forces are analyzed at a fixed Froude number of $Fr = 0.4$ and for submergence depths at $h = 0.25, 0.5, 0.75$. A comparison of the present results with the case in the absence of a free surface is also included to illustrate the effects of inclusion of a free surface. The code validation in special cases shows good comparisons with previous numerical and experimental results. Flow regime analyses include free surface physics-based analysis, and results confirm findings of a recent work of Brøns et al. [25].

1 Introduction

Fluid flow of an infinite extent around oscillating bluff bodies has been studied previously in hundreds of papers owing mainly to its practical significance (see e.g., [1–6] and book chapters in [7–11]). However, relatively few research has been undertaken to investigate the interaction of a free surface wave motion with moving cylindrical bodies (see e.g., [12–17]). Only few numerical studies investigated the interaction of a viscous nonlinear free surface wave motion with moving cylindrical bodies [15–17].

This paper presents numerical results of flow past a streamwise oscillating cylinder beneath a free surface based on a two-fluid model. This model involves the fluids in the regions Ω_1 and Ω_2 with densities, ρ_1, ρ_2, and dynamic viscosities, μ_1, μ_2, entering into

[a] e-mail: serpil@mun.ca

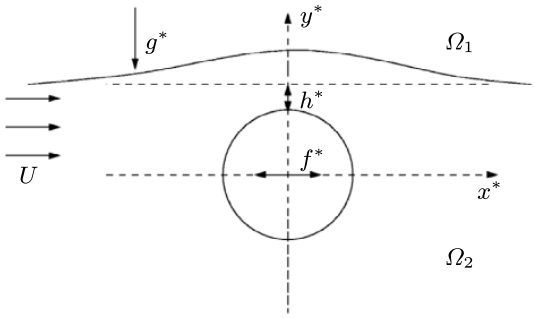

Fig. 1. Schematic of the problem.

the domain with uniform velocity U at the inlet and leaving through the outlet boundary as shown in Fig. 1. The circular cylinder of radius, d, is submerged in the fluid region, Ω_2, at the distance h^* below the undisturbed free surface. Initially, an infinitely long circular cylinder whose axis coincides with the z-axis is at rest, and then, at time $t = 0$, the cylinder starts to perform streamwise oscillations about the x-axis. The imposed oscillatory cylinder displacement is assigned by $x(t) = A\cos(2\pi ft)$. The relevant dimensionless parameters are the Reynolds number $R_2 = Ud/\nu_2$ ($R_1 = Ud/\nu_1$); the forcing amplitude of the cylinder oscillations, $A = A^*/d$; the frequency ratio, f/f_0, with $f = df^*/U$ and $f_0 = df_0^*/U$ being the dimensionless forcing frequency of the cylinder oscillation and the natural vortex shedding frequency for the corresponding stationary cylinder case in an unbounded medium; the cylinder submergence depth, $h = h^*/d$, and the Froude number, $Fr = U/\sqrt{dg^*}$. Here, $\nu_1 = \mu_1/\rho_1$, $\nu_2 = \mu_2/\rho_2$ are the kinematic viscosities of the fluids in Ω_1 and Ω_2, respectively, f^* is the dimensional forcing frequency of cylinder oscillation, f_0^* is the dimensional natural vortex shedding frequency of a stationary cylinder, g^* is the acceleration due to gravity, $\mathbf{g}^* = (0,\ g^*,\ 0)$, $t^* = td/U$ is the dimensional time, and t being the dimensionless time. The dimensionless fluid pressure, p, is defined by $p/\varepsilon = p^*/\rho_2 U^2$, where $\varepsilon = \rho_1/\rho_2$ when $\mathbf{x} \in \Omega_1$, and $\varepsilon = 1$ when $\mathbf{x} \in \Omega_2$.

In order to achieve a fixed grid with respect to the cylinder, it is necessary to use a non-inertial frame attached to the cylinder. The same coordinates and reference frame as those employed by Mironova [16] and Bozkaya et al. [17], are used. Thus, the governing equations and boundary conditions remain unaltered and will be summarized briefly below. In the present two phase flow model governing equations are the two-dimensional continuity and the Navier-Stokes equations given by

$$\frac{d\mathbb{V}}{dt} + \int_{\mathbb{A}} (\mathbf{u}\cdot\mathbf{n})\mathrm{d}S = 0, \tag{1}$$

$$\frac{d}{dt}\int_{\mathbb{V}} u\mathrm{d}V + \int_{\mathbb{A}} (\mathbf{n}\cdot\mathbf{u})u\mathrm{d}S = -\frac{1}{\varepsilon}\int_{\mathbb{A}\cup\mathbb{I}} pn_1\mathrm{d}S + \frac{1}{R}\int_{\mathbb{A}\cup\mathbb{I}} \mathbf{n}\cdot\nabla u\mathrm{d}S + \int_{\mathbb{V}} -a_1\mathrm{d}V, \tag{2}$$

$$\frac{d}{dt}\int_{\mathbb{V}} v\mathrm{d}V + \int_{\mathbb{A}} (\mathbf{n}\cdot\mathbf{u})v\mathrm{d}S = -\frac{1}{\varepsilon}\int_{\mathbb{A}\cup\mathbb{I}} pn_2\mathrm{d}S + \frac{1}{R}\int_{\mathbb{A}\cup\mathbb{I}} \mathbf{n}\cdot\nabla v\mathrm{d}S + \int_{\mathbb{V}} \frac{1}{Fr^2} - a_2\mathrm{d}V, \tag{3}$$

where $\mathbb{V}$ and $\mathbb{A}$ are the fractional volume and area, respectively, open to flow within the computational cell, V; $\mathbb{I}$ is the length of the fluid-body interface open to flow; $\mathbf{u}$ is the dimensionless velocity vector, where $\mathbf{u} = (u, v, 0)$; $\mathbf{n}$ is the outward unit normal vector; S is the control volume boundary. These dimensionless quantities

are defined in terms of their dimensional counterparts: $x = x^*/d$, $y = y^*/d$, $u = u^*/U$, $v = v^*/U; V = V^*/d^2$, $S = S^*/d$, $\mathbb{V} = \mathbb{V}^*/d^2$, $\mathbb{A} = \mathbb{A}^*/d$, $\mathbb{I} = \mathbb{I}^*/d$. The external force, $\mathbf{F} = (-a_1, 1/Fr^2 - a_2, 0)$, is due to the dimensionless gravity force, $\mathbf{g} = (0, 1/Fr^2, 0)$, and the dimensionless acceleration of the non-inertial frame of reference, $(-a_1, -a_2, 0)$. The single set of governing Eqs. (1)–(3) are solved in the flow part of the computational domain, $\Omega = \Omega_1 \cup \Omega_2$, after setting the fluid properties to ρ_1/ρ_2=1/100 and μ_1/μ_2=1/100 (or ν_1/ν_2=1) following the work of Reichl et al. [15]. Therefore, the Reynolds numbers in the fluid regions Ω_1 and Ω_2 are the same ($R \equiv R_1 = R_2$) which is varied by altering the viscosity.

The boundary conditions for the problem under consideration are no-slip of the fluid on the cylinder surface, $u = 0$, $v = 0$; the uniform stream at the inflow, $u = U - v_1$, $v = -v_2$; and the free slip conditions at the top and bottom boundaries of the computational domain, $\partial u/\partial x = 0$, $v = -v_2$. The well-posed open boundary conditions,

$$\frac{1}{R}\frac{\partial u}{\partial x} + \frac{\bar{h}}{Fr^2} = p, \quad \frac{\partial v}{\partial x} = 0 \tag{4}$$

are enforced at the outflow boundary. Here, v_1 and v_2 are the x- and y-components of the velocity of the non-inertial frame of reference, respectively, and $\bar{h}$ is the height of the fluid at the outflow boundary. The uniform flow is used as the initial condition. It is assumed that at time $t = 0$, the free surface is undisturbed.

2 Method of solution and validation

The continuity and Navier-Stokes equations are discretized using a finite volume approximation for two fluid regions Ω_1 and Ω_2 on a fixed Cartesian grid. This is done based on the aggregated-fluid approach by describing the behaviour of both fluids using one set of Eqs. (1)–(3). In this approach the free surface is no longer the boundary of the calculation domain but just the interface between two fluids. A second-order accurate central-difference scheme is used to discretize the governing equations in space in conjunction with first-order explicit forward Euler scheme to advance the numerical solution in time. A cell merging procedure is used to preserve a global second-order accuracy of the spatial discretization. The present paper adopts basically the same numerical method of solution as that used by Mironova [16] and Bozkaya et al. [17], and only a brief description of points of direct relevance to the computations will be provided here.

The main computational difficulty is solving the governing equations in an inertial frame of reference which results in pressure spikes. When the cylinder moves through the fixed staggered grid the pressure cell which belongs to the cylinder at the time instant t_1 may become the fluid cell at the next time instant t_2 where the continuity equation needs to be discretized. Since at the time instant t_1 the velocities in the pressure cell do not satisfy the continuity equation exactly, the pressure field has to do extra work to restore mass balance in the pressure cell at the time instant t_2. This problem was unsuccessfully attempted to overcome in previous numerical studies. This extra work reflects as a spike in the pressure. In the present study, this problem is eliminated by employing a non-inertial frame of reference. The free surface interface is discretized with the volume-of-fluid method due to Hirt and Nichols [18]. Its advection in time is performed based on the strictly mass conserving volume-of-fluid advection method in two dimensional incompressible flows, due to Aulisa et al. [19]. For the moving fluid-body interface the fractional area/volume obstacle representation method due to Hirt and Sicilian [20], and the cut cell method due to Gerrits [21] are employed.

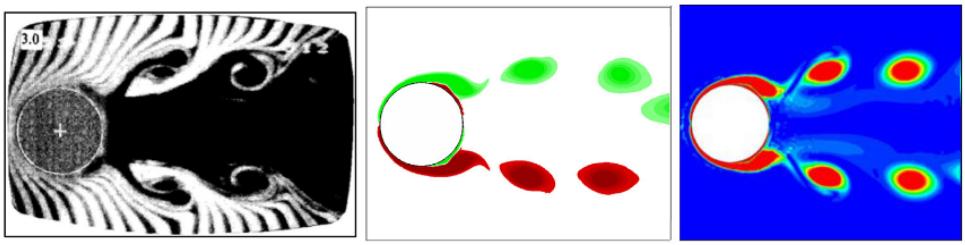

Fig. 2. Comparison of the vorticity field: flow visualization of Ongoren and Rockwell [1] (left), present computation (middle), computation of Do et al. [5] (right) for the case of streamwise oscillating cylinder ($h = \infty$) at $R = 855$, $A = 0.13$ and $f/f_0 = 3.0$.

The present unsteady flow calculations are carried out based on the grid system $L_1(= 20) \times L_2(= 30) \times L_3(= 40)$ with 252×196 elements. The computational grid geometry is defined with respect to the mean position of the cylinder and by specifying the locations of inflow and outflow boundaries, L_1 and L_2, along the x-axis and the location of the top and bottom boundaries, L_3, along the y-axis. In the vicinity of the mean cylinder position, the grid has fine resolution and is uniform. Outside of the uniform grid region, the grid expands exponentially towards the four boundaries of the computational domain. The computational domain size and the number of cells per diameter are the same as that used by Mironova [16] and Bozkaya et al. [17]. Unless otherwise stated, the computations for $R = 200$ are terminated at $t_{\max} = 100$ and 150 (time step: $\Delta t = 0.005$), in the presence and absence of a free surface (symbolically $h = \infty$), respectively. The predicted natural vortex shedding frequency at $R = 200$ is $f_0 = 0.198$. The present numerical algorithm is validated for the cases of uniform flow past a stationary cylinder and a streamwise oscillating cylinder. Tests are conducted in the case of a stationary cylinder at $R = 200$ and using the numerical grid with $L_1 = 20$, $L_2 = 30$, $L_3 = 40$; 60 cells per cylinder diameter and $\Delta t = 0.0075$; the predicted natural shedding frequency, $f_0 = 0.197$, and the predicted values of the mean drag coefficient, $\widehat{C_D} = 1.331$ and the maximum lift coefficient, $C_{L,max} = 0.681$, are in good agreement with the previous numerical and experimental studies by Poncet [22], and Wen and Lin [23], respectively.

The predicted values of maximum lift coefficient $C_{L,max} = 0.92$ and the mean drag coefficient $\widehat{C_D} = 1.70$, for the case of streamwise oscillating cylinder at $R = 100 : A = 0.14, f/f_0 = 2.0$ are compared with the numerical results of Su et al. [24] ($C_{L,max} = 0.97$, $\widehat{C_D} = 1.70$). The results show good agreement. Verification of force coefficients is also made for the case of streamwise oscillating cylinder at $R = 175 : A = 0.14, f/f_0 = 1.4$. The present results ($C_{L,rms} = 0.659$, $\widehat{C_D} = 1.354$) and the numerical results of Leontini [6] ($C_{L,rms} = 0.664$, $\widehat{C_D} = 1.384$) are in good agreement. Figure 2 shows the comparison of the near-wake structure obtained in the present study for the case of streamwise oscillating cylinder at $R = 855, A = 0.13$ and $f/f_0 = 3.0$ with the experimental visualization [1] and the computed wake structure [5]. This figure shows good qualitative agreement between the present computed near-wake structures and those obtained in [1] and [5].

In order to ensure that chosen values of L_1, L_2, L_3 are sufficient to predict free surface flow properties accurately, further tests are conducted for uniform flow past a stationary cylinder in the presence of a free surface at $R = 200 : Fr = 0.3, h = 0.55$. The flow is simulated up to $t = 120$ and is quasi-periodic over this interval of time. The maximum and minimum local heights of the free surface, $h|_{L,max}$ and $h|_{L,min}$; the root mean square value of the lift coefficient, $C_{L,rms}$; the root mean square value of the drag coefficient, $C_{D,rms}$; the natural vortex shedding frequency in the presence

of a free surface, $f|_{fs}$, are calculated using the grid with $L_1 = 20$, $L_2 = 30$, $L_3 = 40$; 60 cells per cylinder diameter. The maximum and minimum local heights of the free surface are measured at time when lift coefficient reaches its maximum. The resulting values are accurate to maximum 3% error when compared to the reference grid with the computational domain size $30 \times 40 \times 60$. This level of accuracy is assumed to be sufficient for the present study. The near-wake grid resolution tests are conducted for uniform flow past a stationary cylinder in the presence of a free surface at $R = 200 : Fr = 0.3, h = 0.7$ using three different grids with 90, 60, 40 cells per diameter for the computational domain $20 \times 30 \times 40$ and the time step, $\Delta t = 0.005$. Results indicate that increasing the number of cells per cylinder diameter from 60 to 90 has a negligible effect on computed quantities f_0, $C_{L,max}$, $C_{D,max}$ and C_D. The grid resolution of 40 cells per diameter gives maximum 1% error in the computed quantities when compared to those with grid resolution of 90 cells per diameter. The grid resolution of 60 cells per diameter is chosen for the current investigation. The sensitivity of the accuracy of computations to the value of the time step is tested using the same grid for three different values of the time steps, $\Delta t = 0.005, 0.0075, 0.01$, for the case of uniform flow past a stationary cylinder in the presence of a free surface at $R = 200$: $Fr = 0.3$, $h = 0.7$. Results with grid resolutions of $40, 60, 90$ indicates that increasing the time step from $\Delta t = 0.005$ to $\Delta t = 0.0075$ to $\Delta t = 0.01$ has a negligible effect (the maximum error is 0.6%) on the computed quantities ($C_{L,rms}$, $C_{D,rms}$, $f|_{fs}$) when compared to the results obtained with the time step $\Delta t = 0.005$: (0.707, 1.564, 0.210) $\rightarrow$ (0.711, 1.564, 0.208) $\rightarrow$ (0.711, 1.564, 0.206).

3 Results

The effects of the free surface inclusion at $h = 0.25, 0.5, 0.75$ and $f/f_0 = 1.5, 2.5, 3.5$ on the flow regimes, vortex shedding modes and their periods, T_v are analyzed ($R = 200$, $A = 0.13$, $Fr = 0.4$). Results are summarized in Table 1. Oscillation amplitude A is maintained at 0.13 since flow structure in such cases for $R = 200$ is characterized by the formation of vortex pairs which convect away from the body, in the absence of a free surface, forming wakes. In general, the effect of the decrease of oscillation amplitude is to reduce the size of the separated region. However, for sufficiently small oscillation amplitude range, $A \ll 1$, when no flow separation takes place, we have the unexpected result that jets issue from the cylinder surface following a boundary-layer collision for the case of purely translational oscillations of a cylinder placed in a quiescent viscous flow. It is also noted that the Froude number, Fr, is (the square root of) the ratio of inertia to gravity, and, since it compares a given characteristic flow velocity to that of (long-wavelength) gravity waves, it directly relates to the speed of a free-surface disturbance. In the present study, free-surface disturbance effects are examined on the fluid forces at $Fr = 0.4$. The free surface deformations at Froude number, $Fr = 0.4$, are considerably larger than the low Froude number cases ($0 < Fr < 0.3$), and results in different vortex shedding modes than low Froude number cases (see p. 346, present study: Table 1, $Fr = 0.4$ and p. 4794, [17]: Table 5, $Fr = 0.2$). At $Fr = 0.4$, as h decreases to 0.25, the localized interface sharpening and wave breaking occur unlike the low Froude number case, $Fr = 0.2$ (see p. 349, present study: Fig. 4, $Fr = 0.4$ and p. 4793, [17]: Fig. 9, $Fr = 0.2$).

Table 1 shows that it is possible to generate distinctly different vortex formation modes than that of the classical modes, observed by Williamson and Roshko [2]. These modes are the combination of the two and three **2S** (or **C**(**2S**)) modes i.e., **4S** (or **C**(**4S**)) and **C**(**6S**) modes. In addition formation of **C**(**2S**) + **S** mode is observed. The asymmetric **2S** mode corresponds to the classical Kármán vortex street which is characterized by single vortices being alternately shed from each side of the cylinder

Table 1. The effect of the free surface inclusion on vortex shedding modes and their periods, T_v, for the case $Fr = 0.4$ and $h = 0.25$, 0.5, 0.75, ∞ at $R = 200$: $A = 0.13$, $f/f_0 = 1.5$, 2.5, 3.5. The superscript "*" denotes quasi-locked-on modes.

	$h = 0.25$		$h = 0.5$		$h = 0.75$		$h = \infty$	
f/f_0	Mode	T_v	Mode	T_v	Mode	T_v	Mode	T_v
1.5	**[C(2S)+S]*** $12T \le t \le 18T$; non-locked $19T \le t \le 29T$;	$2T$ –	**4S*** $T \le t \le 20T$; non-locked $21T \le t \le 29T$;	$3T$ -	**4S*** $2T \le t \le 16T$; non-locked $17T \le t \le 29T$	$3T$ –	**2P**	$2T$
2.5	**[C(2S)+S]*** $11T \le t \le 28T$; non-locked $29T \le t \le 49T$	$3T$ –	**C(6S)*** $5T \le t \le 33T$; non-locked $34T \le t \le 49T$	$7T$ –	**C(6S)*** $2T \le t \le 17T$; non-locked $18T \le t \le 49T$	$7T$ –	**C(6S)***	$8T$
3.5	**[C(2S)+S]*** $16T \le t \le 31T$; non-locked $32T \le t \le 69T$	$5T$	**C(4S)*** $7T \le t \le 40T$; non-locked $41T \le t \le 68T$	$7T$	**C(4S)*** $5T \le t \le 22T$; non-locked $23T \le t \le 69T$	$7T$	**C(2S)*** $50 \le t \le 71T$; non-locked $72T \le t \le 104T$	$4T$

per cycle. The mode $\mathbf{C(2S)} + \mathbf{S}$ is similar to $\mathbf{C(2S)}$ mode with an additional single vortex, **S**, shed from the free surface: coalescence, **C**, between positive vortices from lower side of the cylinder occurs and the development of positive vorticity near the curved free surface is also observed. The mode **C(2S)** results from smaller vortices coalesce directly behind the cylinder forming the **2S** mode near the cylinder or the **2S** mode forms in the near wake region, but further downstream smaller vortices coalesce. Table 1 shows that the presence of the free surface at $h = 0.25$ seems to cause a switchover in the vortex shedding modes when compared to reference case $h = \infty$. That is, the vortex shedding, $\mathbf{C(2S)} + \mathbf{S}$, mode is observed at $h = 0.25$, per $2T$, and, per $3T$, when $f/f_0 = 1.5$ and $f/f_0 = 2.5$, respectively, whereas the locked-on **2P** mode, per $2T$, for $f/f_0 = 1.5$ and the quasi-locked-on **C(6S)** mode, per $8T$, for $f/f_0 = 2.5$ are seen in the absence of free surface ($h = \infty$). In **2P** mode two pairs of vortices shed from both sides of the cylinder per cycle. Furthermore, at the highest frequency ratio, $f/f_0 = 3.5$, a switchover from the quasi-locked-on $\mathbf{C(2S)}$ mode, per $4T$, to the quasi-locked-on $\mathbf{C(2S)} + \mathbf{S}$ mode, per $5T$, occurs as h decreases from ∞ to 0.25. As the cylinder submergence depth, h, increases the flow behaviour becomes more complicated and hence different vortex shedding modes develop depending on the frequency ratio, f/f_0. A switchover in the vortex shedding modes occurs as the frequency ratio increases from 1.5 to 3.5 in the presence of the free surface at $h = 0.5$, 0.75. It is important to note that flow becomes periodic (or quasi-periodic) over several periods of cylinder oscillation, and then a transition into the non-periodic state occurs. A switchover in the vortex shedding modes occurs when $h = 0.5$, 0.75, ∞ as the frequency ratio, f/f_0, increases. However, an increase in h from 0.5 to 0.75 has no effect on the vortex shedding modes for each f/f_0. Similar phenomena has been reported in the experimental study by Cetiner and Rockwell [13] for the case of cylinder subject to streamwise oscillations in uniform flow in the presence of the free surface. Cetiner and Rockwell have shown that at certain Fr-h combinations, the presence of the free surface causes a switching between the near wake states. This study also reported that the vortex shedding exhibits locked-on (or quasi-locked-on) states at least over several cycles of cylinder oscillations and then, the transition to the non-locked-on state occurs.

The detailed analysis of the new vortex shedding mode, $\mathbf{C(4S)}$, per $3T$ will be given only for the frequency ratio, $f/f_0 = 1.5$, when $h = 0.5$. Figure 3 displays the

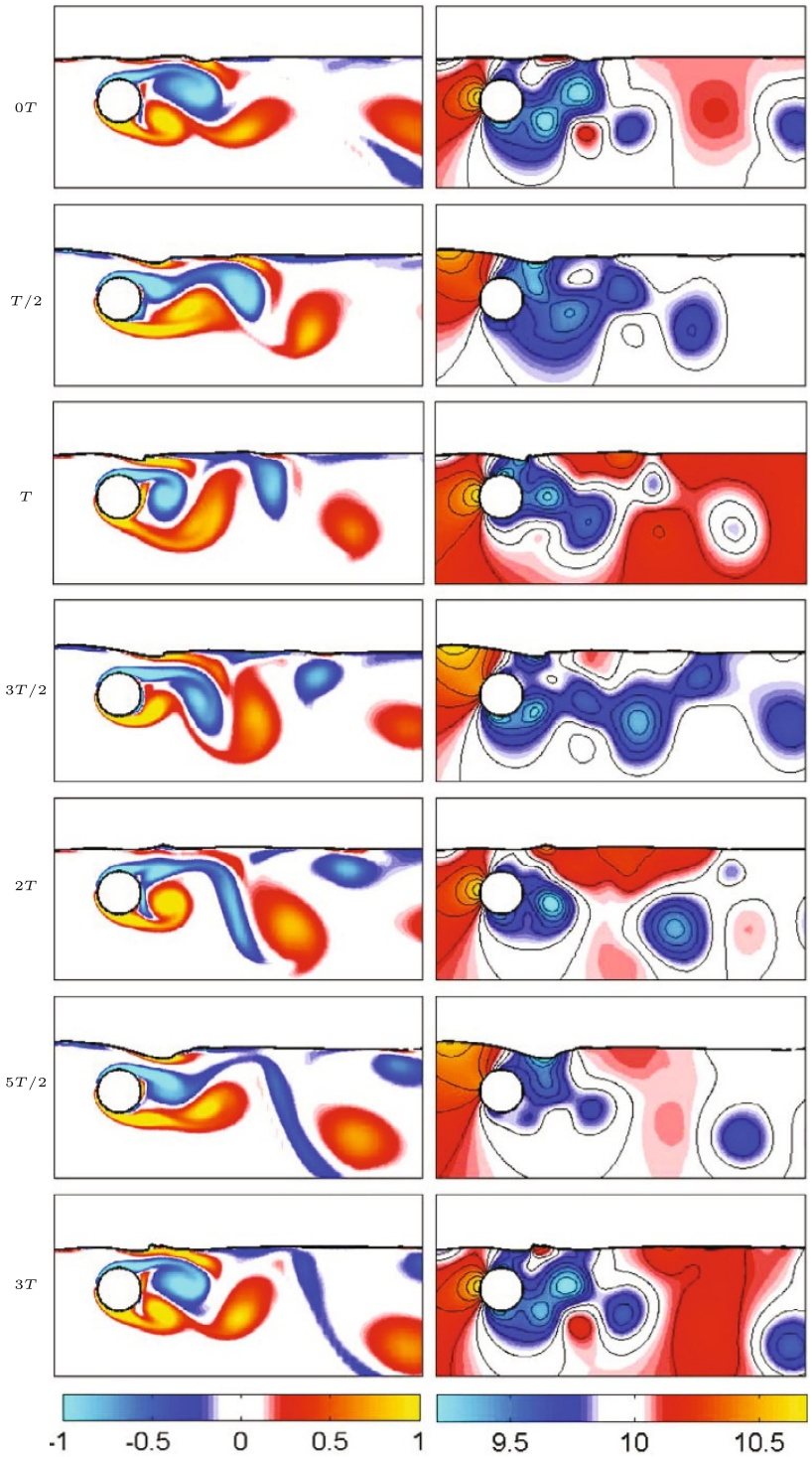

Fig. 3. The equivorticity patterns (left) and the pressure contours (right) in the near wake over three periods of cylinder oscillation, $3T$, at $R = 200$: A=0.13, $f/f_0 = 1.5$ when $Fr = 0.4$ and $h = 0.5$ [$T \approx 3.367$, $26.936 \leq t \leq 37.037$: $(8T, 11T)$]. The quasi-locked-on **4S** mode, per $3T$, is observed ($t \leq 20T$).

equivorticity and the pressure contours in the near wake over three periods of cylinder oscillation, $3T$, for the case $Fr = 0.4$, $h = 0.5$, when $f/f_0 = 1.5$ (quasi-periodic state). In the equivorticity plots, red colours correspond to positive (counterclockwise rotation) and blue colours indicate negative (clockwise rotation) vortices. The vortex shedding mode is the quasi-locked-on **4S** mode, per $3T$, within $20T$. This mode is the combination of the two classical **2S** modes. The flow becomes non-periodic within $21T \leq t \leq 29T$. The cylinder sheds alternately positive and negative vortices (developed in the previous vortex shedding cycle) from lower and upper sides at $t \approx T/2$ and $t \approx T$, respectively. At $t = 3T/2$, the positive vortex (lower side of the cylinder) attaches to the elongated positive vortex from the free surface, and envelops the negative vortex (upper side of the cylinder). The cylinder then sheds the positive vortex and the elongated negative vortex at $t \approx 2T$ and $t \approx 3T$, from the upper and lower sides of the cylinder, respectively; the positive surface vorticity separates into the flow. The cylinder velocity is at its maximum in each of snapshot of the flow shown in Fig. 3. Snapshots at $t = 0T, 3T/2, 3T$ represent the situation at the beginning, middle and end of the vortex shedding cycle, $T_v(= 3T)$. In Fig. 3, the pressure plots with red colors correspond the high pressure region, and blue colors indicate low pressure region. At $t = 0T$, the lowest pressure region occurs behind the cylinder and the region below the cylinder; and then it switches to the right side of the region directly above the cylinder when the free surface falls down sufficiently in this region (t=5T/2). The high speed, low pressure fluid that flows through the gap between the cylinder and the free surface induces circulation at the free surface interface of sign opposite to that in the separating layer. The surface also deflects downwards towards the low pressure region (at $t = T/2$, $5T/2$) before curving up towards its original height downstream ($t = 2T$ and $4T$ (not shown here)). When the negative vortices are shed from the upper side of the cylinder at $t \approx T$ and $t \approx 3T$, a local free surface rising with positive curvature is observed. This is clearly associated with the significant amount of positive vorticity formation at the free surface interface. The positive surface vorticity separates into the flow ($t \approx 2T$), leading to rapid cross-annihilation of vorticity shed from the cylinder as well as rapid "disappearance" of the surface vorticity as the free surface reaches its original height downstream ($t = 2T$ and $4T$ (not shown here)). Thus, the loss in the fluid region of negative vorticity shed from the cylinder is precisely balanced by the change in the vorticity stored in the interface vortex sheet. Curvature of the free surface is essential for rapid onset separation from it and causes very rapid distortion of the flow pattern, involving a sharp drop in the magnitude of the velocity along the surface. This results in substantial flux of vorticity into the region of fluid downstream. The averaged flux of vorticity in the layer from the free surface must be the same as from the surface of the cylinder i.e., local curvature of the free surface near separation must adjust to a value such that the vorticity flux from the free surface matches to that from the cylinder, which has a fixed curvature (see e.g., Sheridan et al. [12]).

The effects of the free surface inclusion at $h = 0.25, 0.5, 0.75, \infty$ and $f/f_0 = 1.5$, 2.5, 3.5 on the flow regimes, are summarized in Fig. 4. At the smallest frequency ratio, $f/f_0 = 1.5$, the lower vortex shedding layer shows a similar behaviour irrespective of the presence of a free surface. On the other hand, inclusion of the free surface seems to cause a change in the vortex formation from the upper side of the cylinder: the shed negative vortex is lifted upward toward the free surface for each $h = 0.25$, 0.5, 0.75; and attaches to the free surface at $h = 0.25$, at the same frequency ratio, $f/f_0 = 1.5$. For the higher frequency ratios, $f/f_0 = 2.5$, 3.5, the near wake shows a quite similar behaviour at $h = 0.5$, 0.75, when compared to that at $h = \infty$. At the smallest cylinder submergence depth, $h = 0.25$, the near wake is dissimilar to the cases at $h = 0.5$, 0.75, especially for $f/f_0 = 3.5$. At $h = 0.25$, downstream at the free surface interface, negative vorticity is stored which provides balance of vorticity to

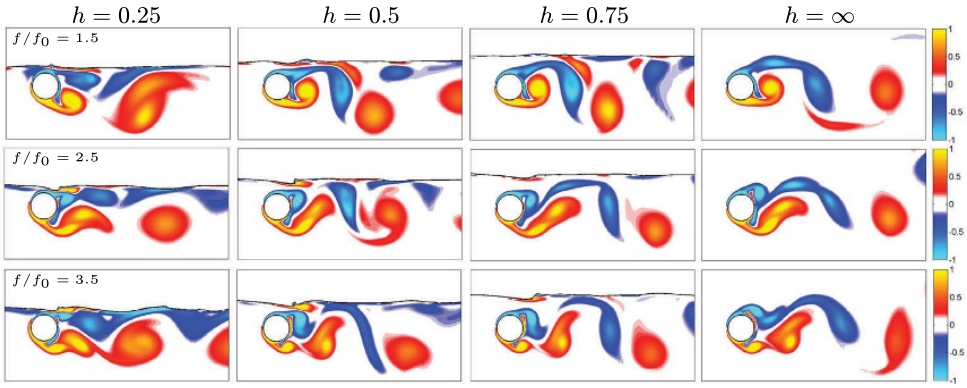

Fig. 4. The effect of the cylinder submergence depth, h, and the frequency ratio, f/f_0, on the equivorticity patterns at $R = 200$: A=0.13, $Fr = 0.4$.

that in the fluid region for all f/f_0. At higher cylinder submergence depths, $h = 0.5$, 0.75, significant amount of vorticity is generated at the curved interface, leading to separation of interface vorticity into the fluid region and rapid cross-annihilation of the negative vortex shed from the cylinder as f/f_0 increases. As the cylinder submergence depth, h, decreases from ∞ to 0.25, the near wake becomes more dominated by positive vortex structures and it seems to be more skew symmetric. The vortex formation length remains almost the same as h decreases from ∞ to 0.25, for all f/f_0, except the case when $h = 0.25$, $f/f_0 = 3.5$. On the other hand, an increase in the frequency ratio, f/f_0, from 1.5 to 3.5 results in an increase in the vortex formation length (maximum by 65.9%) for the cylinder submergence depths, $h = 0.5$, 0.75, ∞. The unsteady development of the fully separated vorticity layer from the free surface occurs relatively independently of the neigbouring layer of opposite vorticity generated from the top surface of the cylinder when the cylinder is at relatively large depths of submergence and a substantial region of irrotational flow exists between two types of layers. In addition, there is a close relationship between the unsteady development of each of the two vorticity layers when the cylinder is relatively close to the free surface. The evolution of small-scale concentrations of vorticity in each of them occurs in a coupled fashion. Numerical experiments at $R = 200$, $A = 0.13$: $f/f_0 = 1.5, 2.5, 3.5$ show that transcritical flow above the cylinder occurs at $h \approx 2.5$ when $Fr = 0.4$.

The time evaluation of the fluctuating lift force, C_L, and the Lissajous patterns, $C_L(x)$, are presented in Figs. 5, 6 for the frequency ratio $f/f_0 = 1.5$ in the absence of the free surface ($h = \infty$) and the presence of the free surface at $h = 0.5$ ($0 \leq t \leq 200$), respectively. For the frequency ratio, $f/f_0 = 1.5$ at the submergence depth, $h = 0.5$, the transition of the flow regime from the quasi-periodic state into the non-periodic state is observed, which is also consistent with the time-dependent behaviour of lift coefficient. The traces of the lift coefficient are almost periodic over three periods of cylinder oscillation, $3T$, within first twenty periods of cylinder oscillation, $20T$, (quasi-periodic state: $T \leq t \leq 20T$); and then they become non-persistent when the switching time is reached at approximately $t = 67.34$; whereas in the reference case $h = \infty$ the traces of C_L show repeatable patterns over $2T$. This observation is also suggested by the corresponding Lissajous patterns. That is, the repeatability of the Lissajous trajectories of C_L in the absence of free surface indicates lock-on between the cylinder motion and the fluctuating C_L. In the presence of free surface at $h = 0.5$, although the Lissajous trajectories of C_L at $f/f_0 = 1.5$ are well-defined, there is a loss of phase-locking confirming that the fluctuating lift coefficient is quasi-phase-locked

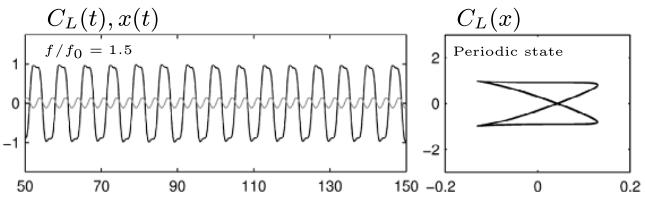

Fig. 5. The time variation of the lift coefficient, C_L, (black) and the streamwise displacement, $x(t)$, (gray); Lissajous patterns of C_L at $R = 200$: A=0.13, $f/f_0 = 1.5$ when $h = \infty$.

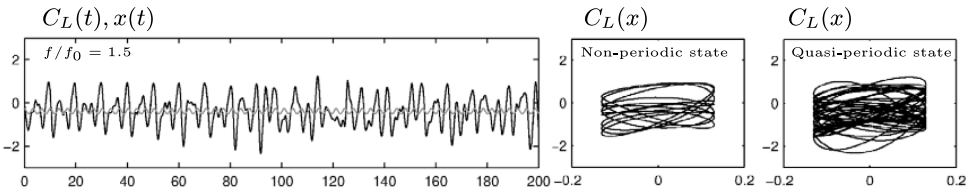

Fig. 6. The time variation of the lift coefficient, C_L, (black) and the in-line displacement, $x(t)$, (gray); Lissajous patterns of C_L at $R = 200$: A=0.13, $f/f_0 = 1.5$ when $Fr = 0.4$ and $h = 0.5$.

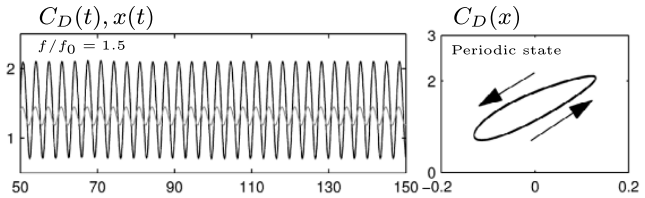

Fig. 7. The time variation of the drag coefficient, C_D, (black) and the in-line displacement, $x(t)$, (gray); Lissajous patterns of C_D at $R = 200$: A=0.13, $f/f_0 = 1.5$ when $h = \infty$.

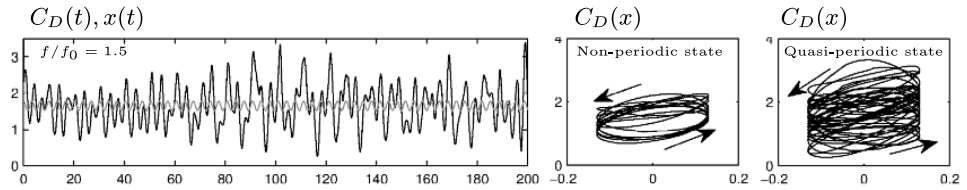

Fig. 8. The time variation of the drag coefficient, C_D, (black) and the in-line displacement, $x(t)$, (gray); Lissajous patterns of C_D at $R = 200$: A = 0.13, $f/f_0 = 1.5$ when $Fr = 0.4$ and $h = 0.5$.

to the cylinder motion (in the quasi-periodic state). In addition, the hysteresis loops are mostly confined in the lower half plane at $h = 0.5$, which shows that the presence of the free surface breaks the symmetry observed in the case when $h = \infty$.

The time history of the drag coefficient, C_D, and the Lissajous patterns of C_D are displayed in Figs. 7, 8 in the absence and the presence of a free surface at $h = 0.5$, respectively. The traces of C_D are non-periodic in the presence of free surface at $h = 0.5$ ($0 \leq t \leq 200$), whereas they show a periodic behaviour in the reference case when $h = \infty$. This is also consistent with the behaviour of the Lissajous patterns of C_D both in the absence and presence of a free surface. Comparison of Fig. 8 with the corresponding ones in Fig. 6 indicates that Lissajous patterns of C_L are consistent with flow behaviour unlike the Lissajous patterns of C_D. That is, the lift coefficient, C_L, has more effect on flow behaviour than the drag coefficient, C_D, when

Table 2. The effect of the free surface inclusion on the mean lift coefficient, $\widehat{C}_L$, for the cases $Fr = 0.4$, $h = 0.25$, 0.5, 0.75, ∞ at $R = 200$: $A = 0.13$, $f/f_0 = 1.5$, 2.5, 3.5.

f/f_0 / h	0.25	0.5	0.75	∞
1.5	$-0.739 \rightarrow -0.858$	$-0.321 \rightarrow -0.408$	$-0.212 \rightarrow -0.212$	-0.000
2.5	$-0.820 \rightarrow -0.970$	$-0.410 \rightarrow -0.398$	$-0.201 \rightarrow -0.290$	-0.001
3.5	$-0.918 \rightarrow -0.961$	$-0.390 \rightarrow -0.478$	$-0.198 \rightarrow -0.324$	$-0.008 \rightarrow 0.025$

Table 3. The effect of the free surface inclusion on the mean drag coefficient, $\widehat{C}_D$, for the cases $Fr = 0.4$, $h = 0.25$, 0.5, 0.75, ∞ at $R = 200$: $A = 0.13$, $f/f_0 = 1.5$, 2.5, 3.5.

$f/f_0/h$	0.25	0.5	0.75	∞
1.5	$1.447 \rightarrow 1.530$	$1.557 \rightarrow 1.698$	$1.609 \rightarrow 1.596$	1.438
2.5	$1.452 \rightarrow 1.512$	$1.606 \rightarrow 1.670$	$1.682 \rightarrow 1.662$	1.373
3.5	$1.422 \rightarrow 1.545$	$1.576 \rightarrow 1.563$	$1.620 \rightarrow 1.701$	$1.349 \rightarrow 1.385$

$h = 0.5$, $f/f_0 = 1.5$. It is also seen that the hysteresis loops are mostly confined in the upper half plane with a counterclockwise direction, indicating that there is a mechanical energy transfer from the cylinder to the fluid regardless of a presence of a free surface. The area enclosed by Lissajous trajectories of C_D at $h = 0.5$ is smaller than that at $h = \infty$, which emphasizes a decrease in the amount of the energy transfer from cylinder to fluid in the presence of free surface at $h = 0.5$.

Tables 2–5 show the effect of the free surface inclusion on the values of the mean lift and drag coefficients, $\widehat{C}_L$ and $\widehat{C}_D$, and the root-mean-square lift and drag coefficients, $C_{L,rms}$ and $C_{D,rms}$, for the cases $Fr = 0.4$: $h = 0.25$, 0.5 and 0.75. Tables 2 and 3 indicate that the presence of the free surface has important consequences for the values of the mean lift and drag coefficients, $\widehat{C}_L$ and $\widehat{C}_D$. Comparison of the results shown in these tables indicates that for $h = 0.25$, 0.5, 0.75 and all values of f/f_0, the values of the mean lift coefficient, $\widehat{C}_L$, are decreased significantly when compared to that at $h = \infty$ in both quasi-periodic and non-periodic states. The $\widehat{C}_L$ varies in the interval between -0.970 and -0.198 when the free surface is present whereas the values of $\widehat{C}_L$ are nearly zero at $h = \infty$, as expected. As the cylinder submergence depth, h, decreases from 0.75 to 0.25, the mean lift coefficient, $\widehat{C}_L$, decreases (by a maximum factor of 4.64) for all frequency ratios, $f/f_0 = 1.5$, 2.5, 3.5.

Table 2 also suggests that the values of $\widehat{C}_L$ change slightly as the transition of the flow from the quasi-periodic state to the non-periodic state occurs. Furthermore, as f/f_0 increases from 1.5 to 2.5, $\widehat{C}_L$ seems to decrease (by a maximum factor of 1.37), except for the cases $f/f_0 = 1.5$, $h = 0.5$ (non-periodic state) and $f/f_0 = 1.5$, $h = 0.75$ (quasi-periodic state). As f/f_0 increases from 2.5 to 3.5, $\widehat{C}_L$ also decreases (by a maximum factor of 1.30), except for the cases $f/f_0 = 2.5$ when $h = 0.5$ (quasi-periodic state), $h = 0.75$ (quasi-periodic state) and $h = 0.25$ (non-periodic state). On the other hand, Table 3 suggests that the presence of the free surface has a slight effect on the values of the mean drag coefficient, $\widehat{C}_D$, for all the values of the cylinder submergence depth, $h = 0.25$, 0.5, 0.75 and the frequency ratio, $f/f_0 = 1.5$, 2.5, 3.5. More precisely, the values of $\widehat{C}_D$ increase by a maximum factor of 1.23 when compared to those at $h = \infty$. On the other hand, as h decreases from 0.75 to 0.25, the values of $\widehat{C}_D$ decrease except for the cases $f/f_0 = 1.5$ and 2.5, $h = 0.5$ (non-periodic state). At the cylinder submergence depths, $h = 0.25$ and $h = 0.5$, the values of $\widehat{C}_D$ seem to increase slightly as the transition of the flow from the quasi-periodic state to the non-periodic state occurs, except the case $f/f_0 = 3.5$, $h = 0.5$. In contrast, for the

Table 4. The effect of the free surface inclusion on the root-mean-square lift coefficient, $C_{L,rms}$, for the cases $Fr = 0.4$, $h = 0.25, 0.5, 0.75, \infty$ at $R = 200$: $A = 0.13$, $f/f_0 = 1.5, 2.5, 3.5$.

$f/f_0/h$	0.25	0.5	0.75	∞
1.5	$0.924 \rightarrow 1.114$	$0.710 \rightarrow 0.861$	$0.744 \rightarrow 0.727$	0.790
2.5	$1.014 \rightarrow 1.215$	$0.741 \rightarrow 0.832$	$0.758 \rightarrow 0.751$	0.454
3.5	$1.015 \rightarrow 1.138$	$0.665 \rightarrow 0.729$	$0.648 \rightarrow 0.716$	$0.427 \rightarrow 0.476$

Table 5. The effect of the free surface inclusion on the root-mean-square drag coefficient, $C_{D,rms}$, for the cases $Fr = 0.4$, $h = 0.25, 0.5, 0.75, \infty$ at $R = 200$: $A = 0.13$, $f/f_0 = 1.5, 2.5, 3.5$.

$f/f_0/h$	0.25	0.5	0.75	∞
1.5	$1.595 \rightarrow 1.673$	$1.621 \rightarrow 1.829$	$1.666 \rightarrow 1.697$	1.521
2.5	$1.797 \rightarrow 1.882$	$2.00 \rightarrow 2.071$	$2.116 \rightarrow 2.112$	2.036
3.5	$2.543 \rightarrow 2.657$	$2.960 \rightarrow 2.970$	$3.155 \rightarrow 3.174$	$3.370 \rightarrow 3.383$

largest cylinder submergence depths, $h = 0.75$ the values of $\widehat{C}_D$ are decreased slightly in non-periodic state. For all cylinder submergence depths, h, $\widehat{C}_D$ seems to increase as f/f_0 increases from 1.5 to 2.5 and to decrease as f/f_0 increases from 2.5 to 3.5 (quasi-periodic state).

Table 4 indicates that the presence of the free surface seems to increase the values of the root-mean-square lift coefficient, $C_{L,rms}$, by a maximum factor of 2.39 except the case $f/f_0 = 1.5$, $h = 0.5$ and 0.75 (quasi-periodic state). Decreasing the cylinder submergence depth, h, from 0.75 to 0.25 seems to increase $C_{L,rms}$ for the cases $f/f_0 = 1.5$, 2.5, 3.5, except $f/f_0 = 1.5$, 2.5 and $h = 0.5$ (quasi-periodic state). It is noted that at $h = 0.25$, 0.5, the values of $C_{L,rms}$ seem to increase slightly as the transition of the flow from the quasi-periodic state to the non-periodic state occurs. However, at $h = 0.75$ the value of $C_{L,rms}$ decrease when the flow is in the non-periodic state for frequency ratios, $f/f_0 = 1.5, 2.5$. The increase in the frequency ratio, f/f_0, from 1.5 to 2.5 seems to increase $C_{L,rms}$ in the presence of the free surface except for the case $f/f_0 = 2.5$ and $h = 0.5$ (non-periodic state). As f/f_0 increases from 2.5 to 3.5 $C_{L,rms}$ decreases for all the values of the cylinder submergence depth, h, in the presence of the free surface. On the other hand, as f/f_0 increases the value of $C_{L,rms}$ decreases when $h = \infty$. Furthermore, taking an overview of Table 5, it is evident that at $h = 0.25$, 0.5, 0.75 and $f/f_0 = 1.5$ the values of the root-mean-square drag coefficient, $C_{D,rms}$, are increased when compared to those at $h = \infty$. However, for $f/f_0 = 2.5$ and 3.5, $C_{D,rms}$ seems to decrease when compared to that at $h = \infty$, except the case when $f/f_0 = 2.5$ and $h = 0.75$ (quasi-periodic state). Decreasing the cylinder submergence depth, h, from 0.75 to 0.25 leads to the decrease in $C_{D,rms}$ for each frequency ratios, f/f_0. Table 5 also suggests that the values of $C_{D,rms}$ increase slightly as the transition of the flow from the quasi-periodic state to the non-periodic state occurs, except for the case $f/f_0 = 2.5$, $h = 0.75$. Finally, it is evident that increasing the frequency ratio, f/f_0, seems to increase the root-mean-square drag coefficient, $C_{D,rms}$ for each cylinder submergence depth, h, shown in Table 5.

4 Conclusion

Two-dimensional flow past a circular cylinder subject to forced streamwise oscillations beneath a free surface is investigated numerically based on a two fluid model. The

numerical simulations are carried out at the Reynolds number of $R = 200$: $A = 0.13$ for three half-integer frequency values, $f/f_0 = 1.5, 2.5, 3.5$. The flow characteristics are examined for Froude number of $Fr = 0.4$ and for the depths of cylinder submergence $h = 0.25$, 0.5, 0.75, ∞. The variations in the cylinder submergence depth, h, and the frequency ratio, f/f_0, have significant effects on flow regimes, vortex shedding modes and fluid forces acting on the cylinder surface. The results show two different flow regimes in the presence of free surface at different combinations of h and f/f_0. Flow becomes periodic (or quasi-periodic) over several periods of cylinder oscillation, and then a transition into the non-periodic state occurs. That is, the inclusion of the free surface seems to stabilize the flow for a short period of time such that the near wake vorticity produces quasi-locked-on modes of vortex shedding and then, the transition of the near wake to the non-periodic state is observed. A similar phenomena has been reported in the experimental study by Cetiner and Rockwell [13] for the case of cylinder subject to streamwise oscillations in uniform flow in the presence of the free surface. On the other hand, in the absence of free surface the flow shows either non-periodic or periodic/quasi-periodic behaviour over the whole time interval after the initial transition period for all f/f_0, except $f/f_0 = 3.5$ in which two flow regimes occur. The resulting new modes are the combination of the two and three **2S** (or **C**(**2S**)) classical modes i.e., **4S** (or **C**(**4S**)) and **C**(**6S**) modes. In addition, the mode **C**(**2S**) + **S**, which is similar to **C**(**2S**) mode with an additional single vortex **S** shed from the free surface, is observed. Flow regime analyses include free surface physics-based analysis, and results of the present study confirm theoretical findings by Brøns et al. [25]. The analysis of the mean and root-mean-square lift and drag coefficient displays that the free surface inclusion has a significant effect on the mean lift coefficient. The values of $\widehat{C}_L$ significantly decreases at $h = 0.25$, 0.5, 0.75 when compared to $h = \infty$ for which the values are almost zero as expected. On the other hand, the free surface presence slightly changes the values of mean drag coefficient $\widehat{C}_D$ for all f/f_0 when compared to those for $h = \infty$. It is interesting to note that irrespective of the values h and f/f_0, the total mechanical energy transfer is negative, indicating the energy transfer from cylinder to fluid unlike the transverse oscillation case. It is important to note that findings of this study are restricted to the parameter range used in this study.

The financial support for this research is provided by the Natural Sciences and Engineering Research Council of Canada.

References

1. A. Ongoren, D. Rockwell, J. Fluid Mech. **191**, 225 (1988)
2. C.H.K. Williamson, A. Roshko, J. Fluids Struct. **2**, 355 (1988)
3. O. Cetiner, D. Rockwell, J. Fluid Mech. **191**, 192 (1988)
4. Q.M. Al-Mdallal, K.P. Lawrence, S. Kocabiyik, J. Fluids Struct. **23**, 681 (2007)
5. T. Do, L. Chen, J.A. Forrest, J. Tu, Eng. Appl. Comput. Fluid Mech. **5**, 579 (2011)
6. J.S. Leontini, D.L. Jacono, M.C. Thompson, J. Fluid Mech. **730**, 162 (2013)
7. E. Naudascher, D. Rockwell, *Flow-Induced Vibrations, An Engineering Guide* (A.A. Balkema Publisher, The Netherlands, 1994)
8. B.M. Sumer, J. Fredsøe, *Hydrodynamics Around Cylindrical Structures* (World Scientific Publishing Company, UK, 1997)
9. M.M. Zdravkovich, *Flow Around Circular Cylinders Vol. 1. Fundamentals* (Oxford University Press, UK, 1997)
10. P. Anagnostopoulos, *Flow-Induced Vibrations in Engineering Practice* (WIT Press, UK, 2002)

11. M.M. Zdravkovich, *Flow Around Circular Cylinders Vol. 2. Applications* (Oxford University Press, UK, 2003)
12. J. Sheridan, J.-C. Lin, D. Rockwell, J. Fluid Mech. **330**, 1 (1997)
13. O. Cetiner, D. Rockwell, J. Fluid Mech. **427**, 29 (2001)
14. J. Carberry, Wake states of a submerged oscillating cylinder and of a cylinder beneath a free surface, Ph.D. thesis, Monash University, 2002
15. P. Reichl, K. Hourigan, M.C. Thompson, J. Fluid Mech. **533**, 269 (2005)
16. L. Mironova, Accurate computation of free surface flow with an oscillating circular cylinder based on a viscous incompressible two-fluid model, Ph.D. thesis, Memorial University, 2008
17. C. Bozkaya, S. Kocabiyik, L.A. Mironova, O.I. Gubanov, J. Comput. Appl. Math. **235**, 4780 (2011)
18. C.W. Hirt, B.D. Nichols, J. Comput. Phys. **39**, 201 (1981)
19. E. Aulisa, S. Manservisi, R. Scardovelli, S. Zaleski, J. Comput. Phys. **192**, 355 (2003)
20. C.W. Hirt, B.D. Nichols, *A Porosity Technique for the Definition of Obstacles in Rectangular Cell Meshes* (Flow Science, Inc., Los Alamos, New Mexico, 1985)
21. J. Gerrits, Dynamics of liquid-filled spacecraft, Ph.D. thesis, University of Groningen, 2001
22. P. Poncet, J. Fluid Mech. **517**, 27 (2004)
23. C.-Y. Wen, C.-Y. Lin, Phys. Fluids **13**, 557 (2001)
24. S.-W. Su, M.-C. Lai, C.-A. Lin, Comput. Fluids **36**, 313 (2007)
25. M. Brøns, M.C. Thompson, T. Leweke, K. Hourigan, J. Fluid Mech. **758**, 63 (2014)